Evaluation of mass transport effects in a bench-scale FB gasifier designed for kinetic determination

Gómez-Barea A., Ollero P., Fernández-Baco C., Villanueva A., Salvador L.
Chemical and Environmental Engineering Department. Escuela Superior de Ingenieros (University of Seville).
Camino de los Descubrimientos s/n. 41092-Seville. Spain.
Telephone: +34 95 4487223 Fax: +34 95 4461775
e-mail: agomezbarea@esi.us.es

Abstract
This paper assesses transport effects in the determination of char reactivity of a batch-operated atmospheric bench-scale bubbling fluidised-bed (BFB) gasifier. Chemical and physical effects were analyzed by dimensionless parameters derived from a simple two-phase model. These parameters were expressed in terms of observable quantities. In such a form, the transport effects could be captured from direct gas measurements. The experimental data taken from a bench-scale BFB gasifier allowed concluding that the fluid-dynamic interferences do not caused limitation in the experimental conditions tested. Computations confirmed that the reactor could almost be looked upon as a differential reactor. However, kinetic measurements made in tests using char particle sizes above 0.75 mm showed to be strongly controlled by intraparticle diffusional effects, especially at temperatures exceeding 850ºC. Preliminary results explain reasonably well diffusional limitations found experimentally. The present analysis enables to select optimum operating conditions in order to be free, as much as possible, of fluid- dynamic and diffusional effects during the determination of char reactivity.

1. Introduction

As part of the design and optimisation of fluidised-bed (FB) gasification processes, an accurate understanding of char gasification within the FB is essential [1]. This is because the heterogeneous reaction of CO_2 and steam with the char, resulting form the devolatilised carbonaceous feed, is usually rate controlling. Many investigators have investigated char gasification by experiments in typical laboratory apparatus (thermo-balance, muffles, etc). However, it is known that solids and gas mixing in an FB is quite different from that in laboratory devices. In spite of this, few experimental data, carried out directly in a fluidized-bed, are reported for these processes. Normally an FB is not well suited for accomplishing kinetic investigations, due to its complex fluid-dynamic pattern, making it difficult to separate kinetic information from influences of mass transfer and fluid dynamics. In practise, an FB influences kinetic data in three ways [2]: (1) backmixing of the gas phase, (2) mass transfer resistance between the bubble and emulsion phases and (3) segregation of char particles within the emulsion phase. In practise, when experiments in laboratory-scale FB are carried out to determine the kinetics, these complications must be avoided. The objective of this article is to establish correct operating conditions of a lab-scale bubbling FB gasifier to obtain chemical kinetic data isolated from fluid-dynamic and transport interferences.

2. Experimental

Only a summary about the facility and the material used is presented here. Further details can be found in Refs. [3] and [4]**.**

2.1. Feedstock and inert material

Ofite, a subvolcanic rock, was used as inert bed material. Ofite is a silicate with formula $(Ca{\cdot}Mg{\cdot}Fe{\cdot}Ti{\cdot}Al)_2{\cdot}(Si{\cdot}Al)_2O_6$. The ofite used in this study has an average particle size of 750 μm and a particle density of 2620 kg/m^3. The char selected is obtained from wood-matter from pressed-oil stone (WPOS), also called orujillo. The main characteristics of one of the samples used in the gasification tests are shown in Table 1 (Group 3). The char samples were ground in a mortar and after sieving two size ranges were obtained: -1000 to +500 μm, and -2830 to +1410 μm. Approximate mean values associated with each particle size range are 750, and 2100 μm, respectively.

2.2. Apparatus

The FB gasifier consists of three parts, a preheating section (a fixed bed of sand), a reaction (bed) part, and the freeboard. The main body, the fluidized bed, is a refractory-lined stainless steel reactor AISI 316 (26.64 mm ID) with 3 mm wall thickness. The distributor plate drilled with 27 holes with 1 mm internal diameter. The reactor has a total height of 375 mm and has two sections, the bed zone of 26.64 mm ID and the freeboard of 52 mm ID. Bed and freeboard are surrounded by an electrical 6 kW_{th} furnace controlled to maintain the desired reaction temperature (800-950ºC).

2.3. Test measurements and procedure

A batch of approximately 1 g of char is fed in each test at the top of the bed. The gas flows up through the bed and leaves the freeboard section. It passes through a thimble filter to collect entrained particles. The gas sampling point is downstream of the cyclones. The composition of the gas produced (CO, CO_2 in the CO_2-char gasification tests reported here) is measured continuously by a Siemens analyser and the flow rate of the outlet gas is measured by a rotameter. The reactor temperature is controlled by a PID, which manipulates the power input to the electrical furnace.

2.4. Experimental conditions

The experimental conditions are detailed in Table 1 where the variables are listed in five groups. Group 1 represents variable which can be adjusted (within a small range) in an experiment in order to avoid hydrodynamic interferences. They are the gas-flow rate, the amount of char, and the Ofite (inert) inventory. Group 2 lists the main properties of the inert particles, which can, in principle, be selected from each test. Group 3 to 5 represent variables that can not be modified. Group 3 and 4 are fixed by kinetic determination constraints. Finally, Group 5 contains geometrical properties of the rig.

2.5. Treatment of data

The char gasification reaction with CO_2 is given by the Boudouard reaction:

$$\mathrm{C\,(s) + CO_2\,(g) \rightarrow 2\,CO\,(g)} \qquad (1)$$

From the total gas flow rate, $Q_g(t)$ and gas composition analysis, $y_{CO}(t)$ and $y_{CO_2}^{IN}$, the gas conversion is calculated by

$$X_g(t) = \frac{y_{CO}(t)}{2 \cdot y_{CO_2}^{IN}} \tag{2}$$

The instantaneous overall rate of char conversion, $dx_c / dt(t)$ is calculated by putting the rate of disappearance of solid carbon in the char equal to the rate of generation of CO according to Reaction (1). This leads to the following expression

$$\frac{d\,x_c}{d\,t}(t) = \frac{12 \cdot y_{CO2}^{IN}}{22.4 \cdot w_{c0}} \cdot Q_g(t) \cdot X_g(t) \tag{3}$$

where w_{c0} is the initial mass of carbon in the char sample. The carbon conversion is obtained by integrating Eq.(3),

$$x_c(t) = \int_0^t \frac{d\,x_c}{d\,t}(t')\,dt' \tag{4}$$

3. Modeling of hydrodynamic effects

The gasifying agent passes the bed as bubbles and gas flowing through the emulsion phase. Reactions are assumed to occur only in the emulsion phase. For the reaction to take place at the internal surface of the particles, CO_2 has to overcome various resistances in its travel from the bubbles to the reacting sites of these surfaces. The drop in CO_2 concentration affects the actual reaction rate, because the concentration at the reacting sites differs from that of the inlet gas stream. To evaluate the differences between the actual conversion and the conversion that would have been obtained if the concentration in the internal reacting sites of the porous char had been that at the entrance (c_{in}), we define the following global effectiveness factor:

$$\eta_G = \frac{(-R)}{k\,{c_{in}}^n} \tag{5}$$

where a n^{th}-order kinetics has been assumed. η_G depends on the resistances involved during the CO_2 pathway. If the times of the physical transport processes are much smaller than the chemical reaction time, the kinetic measurements are directly valid for building up an expression for char gasification kinetics. However, if any resistance other than the kinetic one is of concern, diffusional effects will be present, and the intrinsic kinetics can not be directly obtained.

3.1. Two-phase fluidised-bed model

A basic two-phase approach has been applied to estimate the CO_2 concentration drop between the inlet c_{in} and the emulsion c_e. The details of the hypothesis made as well as the derivation of the equations below are fully covered elsewhere [3]. A molar balance for the gas in the bubble and emulsion phases in the units (mol $m^{-2} \cdot s^{-1}$) leads to

$$\beta\,u_0\,dc_b = k_b\,\varepsilon_b\,(c_e - c_b)\,dz \quad \text{with I.C. } z = 0 \quad c_b = c_{in} \tag{6}$$

$$(1-\beta)\,u_0\,(c_{in} - c_e) = \int_0^{L_f} k_b\,\varepsilon_b\,(c_e - c_b)\,dz + \varepsilon_c\,(\eta_p k\,c_e^n)\,L_f \tag{7}$$

Where β is dimensionless excess gas velocity, defined by Eq. (19) and η_p is the particle effectiveness factor defined in Eq. (17). The CO_2 concentration at the outlet stream (at $z = L_f$) is the result of the contribution of both bubble and emulsion gas concentrations, thus

$$c_{out} = \beta\, c_b + (1-\beta)\, c_e \tag{8}$$

The gas conversion and the interphasic effectiveness are defined, respectively, as

$$X_g = (1 - c_{out}/c_{in}) \quad \text{and} \quad \eta_{ph} = c_e^n / c_{in}^n \tag{9}$$

3.2. Dimensionless governing parameters

By integrating Eqs. (6)-(7) (see Ref. [3] for details), expressions for η_{ph} and X_g as function of two dimensionless numbers $\mathrm{N_a}$ and $\mathrm{Da_R}$ can be written as

$$\frac{(1 - X_g/\mathrm{N_a})^n}{X_g/\mathrm{N_a}} = \frac{\mathrm{N_a}}{\mathrm{Da_R}} \quad \text{and} \quad \frac{\eta_{ph}}{(1-\eta_{ph}^{1/n})} = \frac{\mathrm{N_a}}{\mathrm{Da_R}} \tag{10}$$

where the dimensionless parameters $\mathrm{Da_R}$ and $\mathrm{N_a}$ are defined as

$$\mathrm{Da_R} = K_v L_f / u_0 \tag{11}$$

$$\mathrm{N_a} = 1 - \beta \exp(-\mathrm{NTU}/\beta) \tag{12}$$

$\mathrm{Da_R}$ is the Damköhler number at reactor scale. It compares the relative importance of gas residence time L_f / u_0 and char reaction time K_v^{-1}. This latter is defined as

$$K_v = \varepsilon_c\, \eta_p k\, c_e^{n-1} \quad (\mathrm{s^{-1}}) \tag{13}$$

The second dimensionless group, the dimensionless concentration $\mathrm{N_a} = (c_{in}-c_{out})/(c_{in}-c_e)$ is based on two parameters: the number of transfer units, NTU and β, which are defined as

$$\mathrm{NTU} = k_b\, \varepsilon_b L_f / u_o \quad \text{and} \quad \beta = (u_o - u_{mf})/u_o \tag{14}$$

In Eq. (13), ε_c is the char hold-up in the bed, while k_b in Eq. (14) is the bubble to emulsion mass-transfer coefficient in $\mathrm{s^{-1}}$. The correlation used is given by Ref. [6],

$$k_b = 2\, u_{mf}/d_b + 5.7 \left(D_g\, \varepsilon_{mf}\right)^{0.5} g^{1/4}/d_b^{1.25} \quad (\mathrm{s^{-1}}) \tag{15}$$

3.3. Dimensionless reactor observable

Equations (10) can not give directly the interphasic effectiveness factor, since the intrinsic kinetics is not known. By combining the two expressions in Eq. (10) the following equation for η_{ph} is obtained

$$\eta_{ph} = \left[1 - \mathrm{X_g/N_a}\right]^n \tag{16}$$

This directly gives the effectiveness factor as a function of gas conversion and $\mathrm{N_a}$. The group $\mathrm{X_g/N_a}$ is an observable, because it is not required to know the intrinsic kinetic constant. $\mathrm{X_g/N_a}$ is directly calculated by measuring the gas conversion and by estimating the number $\mathrm{N_a}$, which is calculated from fluid-dynamic information (see Table 2).

4. Evaluation of transport effects in FB experiments

Figure 1.a. displays the expression given by Eq. (16). More specifically, η_{ph} is presented as a function of the group $\mathrm{X_g/N_a}$ (in %) for various reaction orders, *n*. It is seen that the interphasic effectiveness is over 0.9 for low values of $\mathrm{X_g/N_a}$, (typically below 0.10) and reaction orders up to 1. The larger $\mathrm{X_g/N_a}$, the smaller η_{ph} and so, the higher the fluid-dynamic interaction. For a given gas conversion, the parameter

N_a is the key for the assessment of transport limitations. N_a depends on β and NTU according to Eq. (12). Figure 1.b. displays graphically this relationship. As seen, values of NTU, higher than unity, approximately give N_a > 0.92 for β<0.5 ($u_0 < 2u_{mf}$). However, the experiments in our rig have been carried out at u_0~0.8 m/s with a typical minimum fluidising velocity of u_{mf}~0.2 m/s. This corresponds to β of around 0.75 and NTU needs to be larger than 2.5 to guarantee values of N_a above 0.95.

Typical values of *n* for the gasification reaction at atmospheric pressure ranges between 0.4 and 1 [4]. In this scenario, η_{ph} remains between 0.9 and 1 for X_g/N_a<0.1 as is shown in Figure 1.a. Thus, when the transport of reactant between the bubble and the emulsion can be neglected, i.e. N_a~ 1, gas conversion determines the interphasic effectiveness factor. For instance for *n*=1 and a gas conversion of 0.2 (20%), the typical effectiveness factor is around 0.8. To improve this situation, a plausible measure could be to decrease the relative amount of char to inert in the reactor by decreasing the initial batch of char. This could lead to lower gas conversion, and the FB could be looked upon as a differential reactor. Actually, if N_a is close to unity but the reaction is fast, the interphasic effectiveness would be lower than unity. Only if the combined group N_a / Da_R becomes low enough, the effectiveness would tend to unity, and the transport effects associated with the FB fluid-dynamics would disappear. By establishing a minimum threshold for the interphasic effectiveness, η^*, the gas conversion that would guarantee a effectiveness equal to or higher than η^* should fulfil the criterion $X_g \leq N_a(1-\eta^{*n})$. For the experimental conditions in our rig (see Table 1) N_a ranged between 8 and 12. Consequently, the time for the bubbles to flush out the CO_2 during the passage through the bed was small (~0.015 s) compared with the residence time (~0.14 s). The reason was probably the small bubble size (typically from 5 to 9 mm). Bubble velocities were computed within the range of 0.7-0.8 m/s. Therefore, N_a was very close to unity. In spite of this, as Figure 4 shows, typical gas conversions ranged between 0.03 and 0.12. This leads to interphasic effectiveness factors between 0.90 and 0.98, for reaction orders between 0.8 and 0.4 (typical for biomass char gasification reactions [4]).

Figure 2 presents the experimental curves of gas conversion vs. time for four different tests carried out at a CO_2 partial pressure of 0.20 bar. All the tests were performed under similar fluid-dynamic conditions. There are two curves for each temperature (850ºC and 900ºC), one corresponding to 0.75 mm initial char particle size and another to 2.1 mm char. The curves corresponding to char particle size of 0.75 mm, clearly appear well-defined with a peak at low times and a tail at long times. On the contrary, the curves corresponding to the larger char size (2.1 mm) show noisier shapes. The curves are not sharp and remain flat during a longer period of time. As already discussed, effectiveness factors associated with the hydrodynamic interferences in the conditions presented in Table 1 are around 0.95. This small value does not explain the marked differences found in Figure 2. Thus, we guess that intraparticle transport effects at the boundary layer and inside the porous char particles are responsible for the strong rate limitation found experimentally. To asses these diffusional effects, we define a particle effectiveness factor, η_p as

$$\eta_p = \frac{(-R)}{k_e\, c_e^n} = \eta_e \cdot \eta_i \qquad (17)$$

Then, $\eta_G = \eta_{ph} \cdot \eta_p$ In Ref. [3] a simple approach for calculating these effects are given in detail. Figure 3 displays the different effectiveness factors (interphasic, external, external and global) vs. char particle conversion for two of the tests presented in Figure 2 carried out at 0.20 bar CO_2 partial pressure and 900ºC using 0.75 and 2.1 mm char particle sizes. As seen, the global effectiveness varies with conversion and can be rather low (around 0.65) at 900 ºC for the 2.1 mm char. At higher temperatures, the global effectiveness is practically the same as the intraparticle effectiveness factor. This clearly shows that the overall process is controlled by the diffusion of CO_2 within the porous char particle. On the other hand, intraparticle and interphasic effects contribute similarly to the overall diffusional resistance in experiments carried out with small particle size. However, the global resistance is much smaller than those found at higher particle size. These findings are helpful for a deeper understanding of the processes taking place in a typical test to determine char reactivity. Thus, this work provides guidelines for taking measures to enable correct operation of a lab-scale FB gasifier within a controlled operating region in order to avoid falsified kinetics.

5. Conclusions

This paper deals with the role of transport effects during char reactivity tests in a semi-continuous lab-scale FB gasifier operated in bubbling regime. The results showed that the resistance between phases was not the controlling factor. However, despite gas conversion is relatively low (between 3-12%), the interphasic effectiveness ranged between 0.90-0.98. In such a situation, the actual effectiveness depended almost entirely on the gas conversion attained in the reactor. A criterion has been developed to determine the maximum permitted gas conversion for a given test in order to establish the interphasic effectiveness factor above a critical value. Comparisons made between tests at different char particle size, keeping the fluid-dynamic parameters constant, revealed char particles to be strongly diffusion-limited when using 2.1 mm char. To carry out proper char reactivity tests in the rig presented in this work, gas conversion should be maintained lower than 10%. In addition, use of char particle size above 0.75 mm should be avoided. Otherwise, transport limitations can impede the correct determination of intrinsic reactivity.

Acknowledgements

The authors thank the financial support of the Commission of Science and Technology (CICYT) of Spain. One of us (A.G.) expresses his gratitude for the hospitality extended to him by Prof. Bo Leckner, Dr. Henrik Thunman and Dr. Germán Maldonado at the Department of Energy Conversion of Chalmers University of Technology, Sweden. Stimulating discussion and helpful comments by Bo Leckner are specially recognised.

Nomenclature

Ar	Archimedes number defined by $\mathrm{Ar} = d_p^3 \rho_g \left(\rho_p - \rho_g\right) g / \mu^2$, –
c_{in}	inlet CO_2 concentration, kmol·m^{-3}

c_e CO_2 concentration in the emulsion, kmol·m^{-3}

c_b CO_2 concentration in the bubbles, kmol·m^{-3}

c_{out} outlet CO_2 concentration, kmol·m^{-3}

d_{bm} maximum bubble diameter, m

d_{b0} initial bubble diameter, m

d_b bubble diameter, m

$d_{b,av}$ average (through the bed height L_f) defined by $d_{b,av} = 1/L_f \int_0^{L_f} d_b\, dz$, m

d_s average diameter of Ofite, m

d_p instantaneous average diameter of char particles, m

d_{or} diameter of holes on the distributor, m

$\mathrm{Da_R}$ Damköhler number at reactor scale defined by eq. (11), –

D_g diffusivity of CO2 in the gas mixture, m^2·s^{-1}

D_t bed diameter, m

dx_c / dt carbon conversion rate, s^{-1}

g acceleration of gravity, 9.81 m·s^{-1}

H bed height of the pipe containing the FB, m

k nth-order kinetic constant, (kmol·m^{-3})$^{1-n}$

k_b interchange coefficient for CO_2 between bubble and emulsion, s^{-1}

K_v apparent pseudo-first order chemical kinetic constant in the bed, s^{-1}

l_{or} spacing between adjacent holes on the distributor, m

L_{mf} bed height at minimum fluidisation conditions, m

L_f bed height calculated by $L_f = L_{mf}(1-\varepsilon_b)$, m

n reaction order, –

N_t hole density of the distributor, m^{-2}

$\mathrm{N_a}$ dimensionless number, defined by eq.(12), –

NTU Number of transfer units, defined by Eq. (14), –

p_{in} inlet CO_2 partial pressure, bar.

Q_g gas volumetric flowrate for normal conditions, Nm^3·s^{-1}

Re_{mf} Reynolds number at minimum fluidisation, defined by $\mathrm{Re}_{mf} = d_s \rho_g u_{mf} / \mu$, –

Re_p particle Reynolds number defined by $\mathrm{Re}_p = d_s \rho_g u_0 / \mu$, –

$(-R)$ observed reaction rate, kmol·m^{-3}

Sh Sherwood number, –

Sc Schmidt number, –

T_{in} inlet gas temperature, ºC

t time, s

u_0 superficial velocity, m·s^{-1}

u_b velocity of bubble, m·s^{-1}

u_{br} relative velocity of bubble, m·s^{-1}

u_{mf} minimum fluidisation velocity , m·s^{-1}

w_c instantaneous mass of char inside the FB, kg

w_{c0} initial mass of char inside the FB, kg

w_s inert (Ofite) inventory inside the FB, kg

X_g gas conversion, % or kmol/kmol

x_c char conversion, –

y_{CO} outlet CO gas fraction, –

$y_{CO_2}^{IN}$ inlet CO_2 gas fraction, –

z axial coordinate, m

Greek

β dimensionless parameter. Also coefficient used in Fig.5, –

ε_{mf} porosity at minimum fluidisation conditions, –

ε_b fraction of bubble in bed, m^3 bubble·m^{-3} bed

ε_c char bed hold-up $\varepsilon_c = (1-\varepsilon_{mf})(1-\varepsilon_b)v_c$, m^3 char·m^{-3} bed

η_G global effectiveness, defined in Eq. (5), –

η_{ph} interphase effectiveness factor, –

η_p particle scale effectiveness factor, defined in Eq. (17), –

η_e external effectiveness factor at particle scale, –

η_i internal effectiveness factor at particle scale, –

μ gas viscosity, Pa·s^{-1}

ϕ_s inert particle sphericity, –

v_c bed char hold up $v_c = \left[1+\left(w_s/(w_c\,x_c)\right)\cdot\left(\rho_c/\rho_s\right)\right]^{-1}$, m^3 char· m^{-3} particles

ρ_{c0} initial density of the char particles, kg·m^{-3}

ρ_g gas density, kg·m^{-3}

ρ_p average density of particles (char + inert) in bed, kg·m^{-3}

ρ_s density of inert, kg·m^{-3}

Literature

[1] C. Luo TW, M. Nakamura, S. Uemiya, T. Kojima*. Development of FBR measurement of char reactivity to carbon dioxide at
elevated temperatures. Fuel 2001;80:233.

[2] Bjerle I. EH, Svensson O. Gasification of Swedish Black Shale in the Fluidized Bed. Reactivity in Steam and Carbon Dioxide Atmosphere. Ind. Eng. Chem. Process Des. Dev. 1980;19:345.

[3] Gomez-Barea A, Ollero P, Leckner B. Mass transport effects during determination of gas-solid reaction kinetics in fluidised bed. Submitted to Chemical Engineering Science 2006.

[4] Gómez-Barea A, Ollero P, Fernández-Baco C, Salvador L. Study of diffusional effects during fluidised bed biomass-char gasification reactivity tests. Submitted to Biomass and Bioenergy, 2006.

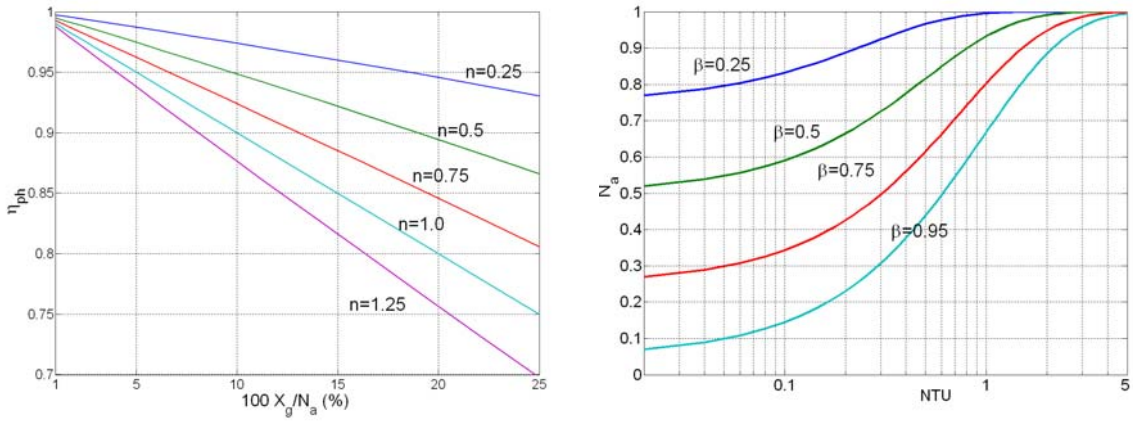

(a) (b)

Figure 1: **(a)** η_{ph} vs. $X_g/\mathrm{N_a}$ for various n**. (b)** $\mathrm{N_a}$ vs. NTU for various β

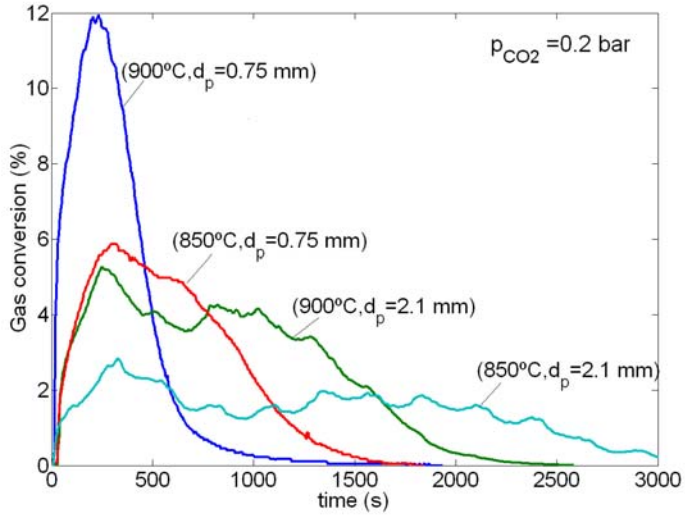

Figure 2: Experimental gas conversion curves for various tests at p_{CO2} =0.20 bar.

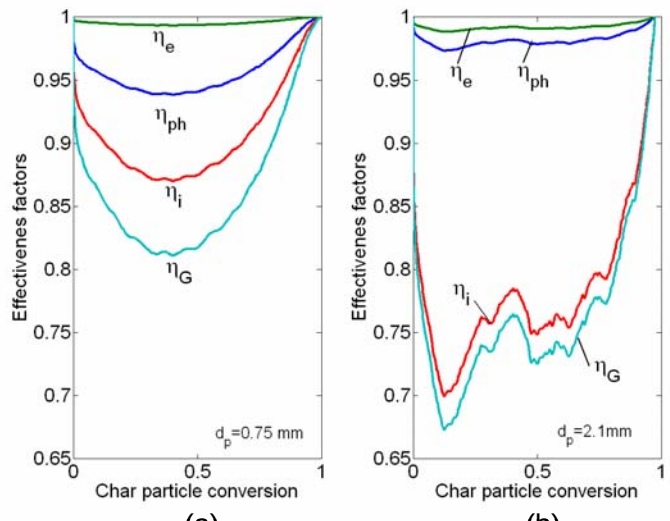

(a) (b)

Figure 3: Effectiveness factors vs. char conversion for the tests at (T= 900ºC, p_{CO2}=0.20 bar) (a) case: d_{p1}=0.75 mm. (b) d_{p2}=2.1 mm.

Table 1. Range of operating condition tested in the experimental rig

Group 1: Q_g = 8.3-9.4·10^{-3} (Nm^3/s) ; w_{c0} = 0.5-2.0 (g); w_s = 10-40(g).
Group 2: ρ_s =2600 (kg/m^3); d_s = 0.75·10^{-3} (m);
Group 3: ρ_{c0} =900 (kg/m^3); d_p = 0.75 - 2·10^{-3} (m);
Group 4: T_{in} = 800-950 (ºC); p_{in} = 0.20, 0.50 (bar)
Group 5: D_t =2.66·10^{-2} (m); N_t = 4.84·10^{-4} (m^{-2}); d_{or} =1·10^{-6} (m); H =0.165 (m);

Table 2. Formula and correlation used in the calculations

Symbol	**Correlation**	**Unit**
u_{br}	$u_{br} = 0.711 \cdot (g \cdot d_b)^{1/2}$	(m·s^{-1})
u_b	$u_b = 1.6 \cdot \left[(u_0 - u_{mf}) + 1.13 \cdot d_{b,av}^{1.35}\right] \cdot D_t^{1.35} + u_{br}$	(m·s^{-1})
d_b	$d_b = d_{bm} - (d_{bm} - d_{b0}) \cdot e^{-0.3 L_f z / D_t}$	(m)
d_{b0}	$d_{b0} = 0.082 / g^{0.2} [(u_0 - u_{mf}) / N_t]^{0.4}$ for $d_{b0} \le l_{or}$ $d_{b0} = 0.0278 / g \cdot (u_0 - u_{mf})^2$ for $d_{b0} > l_{or}$	(m)
d_{bm}	$d_{bm} = \mathrm{Min}\left\{ 163.77 \cdot \left[\pi D_t^4 / 4 \cdot (u_0 - u_{mf}) \right]^{0.4}, D_t \right\}$	(m)
ε_b	$\varepsilon_b = (u_0 - u_{mf}) / (u_b - u_{mf})$	(m)
Sh	$\mathrm{Sh} = 2\varepsilon_{mf} + 0.69 (\mathrm{Re}_p / \varepsilon_{mf})^{1/2} Sc^{1/3}$	-
L_{mf}	$L_{mf} = (w_s + w_c) / (\rho_p (1 - \varepsilon_{mf}) \pi D_t^4 / 4)$	(m)